GEOPHYSICAL RESEARCH LETTERS, VOL. ???, XXXX, DOI:10.1029/,

Internal and forced modes of variability in the Indian Ocean

A. Bracco, F. Kucharski, F. Molteni

The Abdus Salam International Centre for Theoretical Physics,

Physics of Weather and Climate Group, Trieste, Italy

W. Hazeleger and C. Severijns

Royal Netherlands Meteorological Institute, De Bilt, NL

A. Bracco, The Abdus Salam ICTP, Physics of Weather and Climate Group, St. Costiera 11, I-34014 Trieste, ITALY. (annalisa@ictp.trieste.it)

Ocean-atmosphere variability in the tropical Indian Ocean is investigated using observational data and ensemble experiments with a coupled general circulation model. In one ensemble (IO runs) the ocean-model domain is limited to the Indian Ocean and observed sea surface temperatures force the atmospheric model elsewhere. In a second ensemble (TPIO) the coupled domain includes the Tropical Pacific. The IO runs display a coupled mode of variability with several characterists of the Indian Ocean Dipole (IOD), but independent on ENSO (El-Niño Southern Oscillation). Changes in the Walker circulation induced by ENSO are insufficient to trigger IOD events. In the TPIO runs ENSO variability is correlated with the IOD mode as observed. Oceanic processes are responsible for an essential component of ENSO forcing in the Indian Ocean. The ENSO phase conditions the thermocline depth in the Indonesian Throughflow region and in the southeastern IO. TPIO results are in agreement with SODA reanalysis.

1. Introduction

The relationship between ENSO and the recently discovered Indian Ocean Dipole or Zonal Mode (*Saji et al.* [1999]) has been a matter of intense debate in the last few years (*Allan et al.* [2001]; *Baquero-Bernal et al.* [2002]; *Saji and Yamagata* [2003]; *Krishnamurthy and Kirtman* [2003]; *Gualdi et al.* [2003]). In this work we address some of the open issues with a set of coupled numerical experiments suited to examine: a) If an internal mode of variability of the Indian Ocean exists independently of ENSO, and if such a mode is pertinent to the observed variability; b) The relationship between ENSO and the IOD, and the conditions under which it can be properly simulated.

The particular set up of the numerical integrations follows a strategy adopted in other studies (*Yu et al.* [2002]; *Yu and Lau* [2004]; *Huang and Shukla* [2005]), and aims to identify the physical mechanisms responsible for the teleconnections over the tropical Indo-Pacific region, revealing that the ocean plays a major role.

2. Model and simulations

The Coupled General Circulation Model (CGCM) consists of the ICTP atmospheric GCM in its 8-layer configuration and T30 horizontal resolution (*Molteni* [2003]; *Bracco et al.* [2004]), and MICOM (Miami Isopycnic Coordinate Ocean Model) version 2.9 (*Bleck et al.* [1992]), in a regional configuration with 20 vertical levels and $1^o \times 1^o$ horizontal resolution. MICOM is initialized with climatological winter values from Levitus (Levitus et al. 1994). In the IO configuration MICOM is confined to the Indian Ocean from 35S to 30N and from the coast of Africa to 140E. A 2^o-wide zone south of 35S and east of 140E is used to blend ocean model Sea Surface Temperatures (SSTs) to observed values

and subsurface quantities to Levitus monthly climatology. The IO ensemble consists of 10 members forced with observed SSTs from the HadISST dataset (*Rayner et al.* [2003]) for the period 1930-1999 outside the OGCM domain. A random perturbation is imposed on the atmospheric initial state of each member. By definition, all members are forced by the same SSTs in the Tropical Pacific. The last fifty years (1950-1999) are considered in the analysis.

The TPIO integrations include the Tropical Pacific ocean in the region 35S to 30N. Monthly observed SST climatology is prescribed elsewhere. Over the OGCM domain a correction on the SSTs forcing the atmosphere (SST_A) is imposed with the form $SST_A = SST_{cl} + \alpha[SST_O - < SST_O >]$, where α grows linearly from 0 to 1 during a 20 year spin-up period, SST_{cl} represents the observed monthly climatology, SST_O the ocean model SST at a given time, and $< SST_O >$ the ocean model monthly climatology accumulated during the spin-up phase. The model is run for a total of 145 years and the first 45 years are discarded. Two members are analyzed. We performed an analogous integration without correction (reference run). The correction allows for reducing the cold bias of the reference run in the equatorial Pacific (a problem common to several CGCMs) and for obtaining a realistic ENSO amplitude, variability and seasonal cycle.

The difference between the observed and the simulated SST climatology in boreal summer, along with the climatology of the modeled winds at 925 hPa, are shown in Fig.1 for the IO ensemble and the TPIO runs, respectively.

In the following, model winds and SST anomalies are compared respectively with NCEP-NCAR reanalysis (*Kalnay and Coauthors* [1996]) and the HadISST dataset for the period

1950-1999. Simple Ocean Data Assimilation (SODA) products (*Carton et al.* [2000]), available at http://iridl.ldeo.columbia.edu for the period 1958-2002, are used to validate ocean variables.

3. The IO ensemble

The IOD index, defined as the difference of area-averaged SST monthly anomalies (SSTAs) in the western tropical IO (WTIO) (50^o-70^oE, 10^oS-10^oN) and in the south-eastern tropical IO (SETIO) (90^o-100^oE, 10^oS-0^o), is plotted in Fig. 2a for three members of the IO ensemble. In all runs, quasi-biennial oscillations with amplitude $\leq 1.^O$C are intercalated by strong positive events, characterized by very cold anomalies in the SE-TIO region. The atmospheric circulation in each member is forced by the same SSTs outside the ocean model domain, but the IOD time-series are independent. Correlations of the model IOD index with the Niño-3.4 time-series (SSTAs averaged over the Pacific Ocean region 170^o-120^oW, 5^oS-5^oN) are distributed as follows: $-0.11 \leq r \leq 0.13$ when all months of the year are considered, $-0.24 \leq r_{JJA} \leq 0.18$ if the analysis is limited to boreal summer, and $-0.28 \leq r_{SON} \leq 0.04$ in fall (September to November). The reference values, based on HadISST data, are $r = 0.32$, $r_{JJA} = 0.54$ and $r_{SON} = 0.62$. Absolute correlations greater than 0.26 and 0.31 are significant above the 95% and 99% confidence levels according to a t-test assuming one d.o.f per season. Only two members develop a positive IOD during the summer of 1997, when the strongest event of the last 50 years was recorded. Therefore, this model configuration does not represent the observed ENSO-IOD teleconnection.

In the ensemble the variability associated with the IOD index results from an autonomous coupled mode, internal to the Indian Ocean dynamics and not correlated with ENSO. Air-sea feedbacks are crucial for its development. The ocean responds locally to the winds, and remotely with the excitation of Rossby and Kelvin waves, in agreement with previous model results (*Murtugudde et al.* [2000]; *Rao et al.* [2002]; *Gualdi et al.* [2003]). Thermocline anomalies in SETIO during spring precondition the sign of the dipole index for the following summer. Regression maps of modeled SSTs and near-surface winds with the (independent) Niño-3.4 and IOD indices in summer (JJA) are presented in Fig.3c-d. ENSO, in its positive phase, forces an anomalous surface divergence over the Indian continent that weakens the monsoon circulation and the associated rainfall. Wind anomalies are, however, slightly too strong over the Indian continent and very weak over SETIO and Sumatra compared to reanalysis. The SST regression map in Fig.3c shows a weak ENSO signal over the Indian Ocean, with a cooling around Indochina accompanied by excessive precipitations. Such a cooling may be model dependent and related to the absence of air-sea coupling over the Pacific (*Wu and Kirtman* [2004]). On the other hand, both SSTs and wind regressions with the Niño-3.4 index show good agreement with NCEP data during spring (not shown). During positive IOD events anomalous winds strengthen the cyclonic circulation over southern India and upwell cold water anomalies off Sumatra. Wind anomalies south of 5^{o}S are weaker than in the NCEP-NCAR reanalysis, and so is the upwelling; precipitation negative anomalies do not extend into Indonesia and are centered few degrees north of the observed signal (not shown).

Results from the IO ensemble support the existence of an autonomous coupled mode of variability of the Indian Ocean with some characteristic of the observed IOD but independent on ENSO. This model configuration cannot properly represent the observed teleconnections between the Indian and the Pacific ocean, suggesting that changes in the Walker circulation associated with ENSO are not enough to force IOD events. ENSO forcing may be recovered if the subsurface connection between the Indian and the Pacific Ocean is restored (as in *Huang and Shukla* [2005]).

4. The TPIO runs

In the TPIO runs, the Pacific and Indian Ocean are connected also through the oceanic bridge and strong IOD events are often associated with ENSO episodes, as evident from the Niño-3.4 and IOD indices plotted in Fig. 2c. The correlations between the IOD and ENSO are $r = 0.45$, $r_{JJA} = 0.46$ and $r_{SON} = 0.49$ respectively for all months, summer, and fall. [1]

A slightly larger correlation coefficient is found between ENSO and SST anomalies in WTIO ($r = 0.47$), in agreement with HadISST and SODA reanalysis, while ENSO and SSTAs in SETIO are weakly anticorrelated ($r = -0.29$) in the model runs, and do not display a significant correlation in the observations (see *Krishnamurthy and Kirtman* [2003]). In the SETIO region the SSTs are influenced by a surface barrier layer (*Sprintall and Tomczak* [1992]), whose thickness is often below the resolution of the model. The subsurface in SETIO, on the other hand, behaves quite differently (*Rao et al.* [2002]), and the agreement between the modelled results and SODA is extremely good. The analysis of the variability of the 20^o isotherm (Z20), a proxy for the thermocline depth, reveals

that Z20 anomalies in SETIO are significantly anticorrelated with the Niño-3.4 index, both in the model runs ($r = -0.46$) and in SODA ($r = -0.49$). Coefficients do not vary significantly through the year. In SODA, the maximum lag correlation ($r = -0.50$) is found for Z20 anomalies lagging ENSO by one month and during the spring season ($r_{MAM} = -0.51$). In the TPIO runs, for Z20 anomalies lagging ENSO by one month, the average correlation is also $r = -0.50$, and for spring $r_{MAM} = -0.47$. All values are above the 99% significance level, according to a t-test.

The thermocline in SETIO is linked to the Indonesian Throughflow (ITF), as costal Kelvin waves transport the ITF signal in the SETIO region off south Java (*Sprintall et al.* [1999]). ENSO modulates the ITF with weaker (stronger) than normal transport of warm, fresh water from the Pacific to the Indian Ocean during its positive (negative) phase (*Meyers* [1996]). *England and Huang* [2005] provide a detailed validation of the ITF and its variability in SODA, and find it in good agreement with the observations available. In their work, the ITF is calculated as the depth integrated transport over the whole water column at 8^oS between 120^oE-131.5^oE and is anticorrelated with the Niño-3 index (SSTA averaged over 150^oW-90^o, 5^oS-5^oN), with a maximum absolute value of $r = -0.32$ for the ITF lagging ENSO by 9 months. [2] Here we limit our analysis to the subsurface. In SODA the correlation between the Z20 anomalies in the ITF region and the Niño-3.4 index is $r = -0.63$, with maximum correlation $r = -0.66$ for the thermocline depth anomalies lagging ENSO by two months (Fig. 4a). In the model runs (Fig. 4b) the average correlations are $r = -0.63$ at 0 lag and $r = -0.70$ at 2-month lag, respectively. ENSO strongly conditions the subsurface in the SETIO region via the ITF, so that ENSO-

related winds anomalies in spring (*Annamalai et al.* [2003]) may effectively trigger the IOD by upwelling subsurface waters at anomalous temperature, whenever the barrier layer can be eroded. The intensity of the thermocline anomalies is, in most cases, proportional to the strength of the ENSO events.

The TPIO regression maps of winds and SSTAs with the Niño-3.4 and IOD indices ((Fig. 3e-f) show good agreement with reanalysis (Fig. 3a-b) and previous results using global ocean models (*Gualdi et al.* [2003]; *Huang and Shukla* [2005]). The ENSO influence over the Indian Ocean is modulated by the co-occurence of the IOD. The weakening of the monsoon circulation is less evident over the Indian peninsula, and westerly winds along Sumatra strengthen during summer due to cooler than normal subsurface waters upwelled to the surface. In the IOD regression, the wind signal is better positioned and protrudes over Indonesia, and the region of upwelling extends to 10^oS.

5. Summary

In the IO ensemble the Indian Ocean displays an autonomous mode of variability with some characteristics of the observed IOD. Such a mode is independent on ENSO and has a quasi-biennial frequency dictated by the Rossby wave propagation time. Exceptionally strong events, with a preferred variability on a 8-10 years period, are associated to $\geq 5^o$C cold anomalies in SETIO. Interestingly, comparable large anomalies have been recorded by corals from western Sumatra during the Holocene, about 4500 and 6300 years ago (*Abram et al.* [2003]), i.e. during periods of low ENSO activity (*Moy et al.* [2002]).

Today, however, ENSO strongly conditions the initiation and evolution of the IOD. During ENSO the atmospheric bridge over the Indo-Pacific basin insures the initialization of

the IOD mode in late spring, modifying the Walker circulation and generating anomalous winds that favor upwelling or downwelling off Sumatra (*Annamalai et al.* [2003]). Such atmospheric teleconnection, reproduced in both the IO and in the TPIO ensembles, is necessary but not sufficient, as demonstrated by the IO runs. The conditioning of the ocean subsurface temperatures off South Java and Sumatra, via the Indonesian Throughflow, is essential to recover the observed relationship between ENSO and the IOD. A shallower (deeper) than usual thermocline in SETIO and at the ITF is associated to the positive (negative) phase of ENSO. The consequent intensification of SST anomalies in the region of upwelling acts as a positive feedback which reinforces the ENSO-IOD locking in summer and fall.

Notes

1. Correlations in the two TPIO runs have similar values and differences are not statistically significant. Significance has been tested with the jacknife method applied to 50-year long subsampling of the original time-series. Values have been averaged over the two members.
2. In both SODA and our model the ITF flows predominantly via the Makassar Strait, as other passages are closed or not properly resolved. This is, however, in agreement with observations.

References

Abram, N., M. Gagan, M. McCulloch, J. Chappell, and W. Hantoro (2003), Coral reef death during the 1997 Indian Ocean Dipole linked to indonesian wildfires, *Science*, *301*, 952–955.

Allan, R., D. Chambers, W. Drosdowsky, H. Hendon, M. Latif, N. Nicholls, I. Smith, R. Stone, and Y. Tourre (2001), Is there an Indian Ocean Dipole, and is it independent of the El Niño southern oscillations?, *CLIVAR Exchanges*, *6(3)*, 18–22.

Annamalai, H., R. Murtugudde, J. Poterma, S. Xie, P. Liu, and B. Wang (2003), Coupled dynamics over the Indian Ocean: Spring initiation of the zonal mode, *Deep-Sea Res. II*, *50*, 2305–2330.

Baquero-Bernal, A., M. Latif, and M. Legutke (2002), On dipole-like variability of sea surface temperature in the tropical Indian Ocean, *J. Clim.*, *15*, 1358–1368.

Bleck, R., C. Rooth, D. Hu, and L. Smith (1992), Salinity-driven thermocline transients in a wind- and thermocline-forced isopycnic coordinate model of the North Atlantic, *J. Phys. Ocean.*, *22*, 1486–1505.

Bracco, A., F. Kucharski, R. Kallummal, and F. Molteni (2004), Internal variability, external forcing and climate trends in multi-decadal AGCM ensembles, *Clim. Dyn.*, *23*, 659–678.

Carton, J., G. Chepurin, X. Cao, and B. Giese (2000), A Simple Ocean Data Assimilation analysis of the global upper ocean 1950-95. Part I: Methodology, *J. Phys. Ocean.*, *30*, 294–309.

England, M., and F. Huang (2005), On the interannual variability of the indonesian throughflow and its linkage with ENSO, *J. Clim.*, *In press*.

Gualdi, S., E. Guilyardi, A. Navarra, S. Masina, and P. Delecluse (2003), The interannual variability in the tropical Indian Ocean as simulated by a CGCM, *Clim. Dyn.*, *20*, 567–582.

Huang, B., and J. Shukla (2005), On the mechanisms of the interannual variability in the tropical Indian Ocean. Part I: The role of remote forcing from the tropical Pacific, *COLA Tech. Rep.*

Kalnay, E., and Coauthors (1996), The NCEP/NCAR 40-year reanalysis project, *Bull. Am. Meteorol. Soc.*, *77*, 437–471.

Krishnamurthy, V., and B. Kirtman (2003), Variability of the Indian Ocean: Relation to monsoon and ENSO, *Q. J. R. Meteorol. Soc.*, *129*, 1623–1646.

Meyers, G. (1996), Variation of indonesian throughflow and the El Niño-southern oscillation, *J. Geophys. Res.*, *101*, 12,255–12,563.

Molteni, F. (2003), Atmospheric simulations using a GCM with simplified physical parameterizations. I. model climatology and variability in multi-decadal experiments, *Clim. Dyn.*, *20*, 175–191.

Moy, C., G. Seltzer, D. Rodbell, and D. Anderson (2002), Variability of El Niño/southern oscillation activity at millenial timescales during the Holocene epoch, *Nature*, *420*, 162–165.

Murtugudde, R., J. McCreary, and A. Busalacchi (2000), Oceanic processes associated with anomalous events in the Indian Ocean with relevance to 1997-1998, *J. Geophys. Res.*, *105*, 3295–3306.

Rao, A., S. Behera, Y. Masumoto, and T. Yamagata (2002), Interannual variability in the subsurface tropical Indian Ocean, *Deep-Sea Res. II*, *49*, 1549–1572.

Rayner, N., D. Parker, E. Horton, C. Folland, L. Alexander, D. Rowell, E.C.Kent, and A. Kaplan (2003), Global analyses of sst, sea ice, and night marine air temperature since the late nineteenth century, *J. Geophys. Res.*, *108*, doi:10.1029/2002JD002,670.

Saji, N., and T. Yamagata (2003), Structure of SST and surface wind variability during Indian Ocean Dipole mode events: Coads observations, *J. Clim.*, *16*, 2735–2751.

Saji, N., B. Goswami, P. Vinayachandran, and T. Yamagata (1999), A dipole mode in the tropical Indian Ocean, *Nature*, *401*, 360–363.

Sprintall, J., and M. Tomczak (1992), Evidence of barrier layer in the surface layer of the tropics, *J. Geophys. Res.*, *97*, 7305–7316.

Sprintall, J., J. Chong, F. Syamusdin, W. Morawitz, S. Hautala, N. Bray, and S. Wijffels (1999), Dynamics of the south Java current in the indo-australian basin, *Geophys. Res. Lett.*, *26*, 2493–2496.

Wu, R., and B. Kirtman (2004), Impact of indian ocean on the indian summer monsoon-ENSO relationship, *J. Clim.*, pp. 3037–3054.

Yu, J.-Y., and K. Lau (2004), Contrasting Indian Ocean SST variability with and without ENSO influence: A coupled atmosphere-ocean GCM study, *Meteor. Atms. Phys*, pp. doi:10.1007/s00,703–004–0094.7.

Yu, J.-Y., C. Mechoso, J. McWilliams, and A. Arakawa (2002), Impacts of the Indian Ocean on ENSO cycle, *Geophys. Res. Lett.*, *29*, 1204,doi:10.1029/2001GL014,098.

Figure 1. Difference between observed and model SST climatology (shaded) and modeled climatological winds at 925 hPa.

Figure 2. a) IOD index for three members of the IO ensemble, b) 2 × IOD (red) and Niño-3.4 (blue) time series for HadISST data, and c) for 50 years of one of the TPIO integrations.

Figure 3. Regression of SSTs and 925 hPa winds on the Niño-3.4 (top) and IOD indices (bottom) for: a-b) HadISST and NCEP reanalysis; c-d) the IO ensemble; e-f) the TPIO ensemble.

Figure 4. Niño-3.4 index (blue) and 0.1 × Z20 anomalies averaged at 7.5^o-8.5^{o}S, 120^{o}E-131.5^{o}E for a) SODA, b) TPIO run.

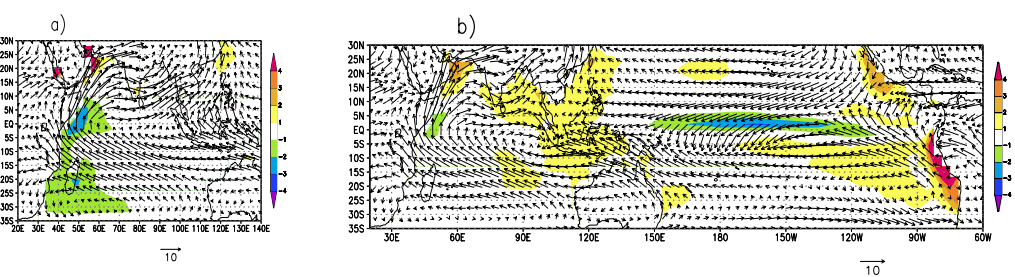
a)
30N
25N
20N
15N
10N
5N
EQ
5S
10S
15S
20S
25S
30S
35S
20E 30E 40E 50E 60E 70E 80E 90E 100E 110E 120E 130E 140E
4
3
2
1
-1
-2
-4
10
b)
30N
25N
20N
15N
10N
5N
EQ
5S
10S
15S
20S
25S
30S
35S
30E 60E 90E 120E 150E 180 150W 120W 90W 60W
4
3
2
1
-1
-2
-4
10

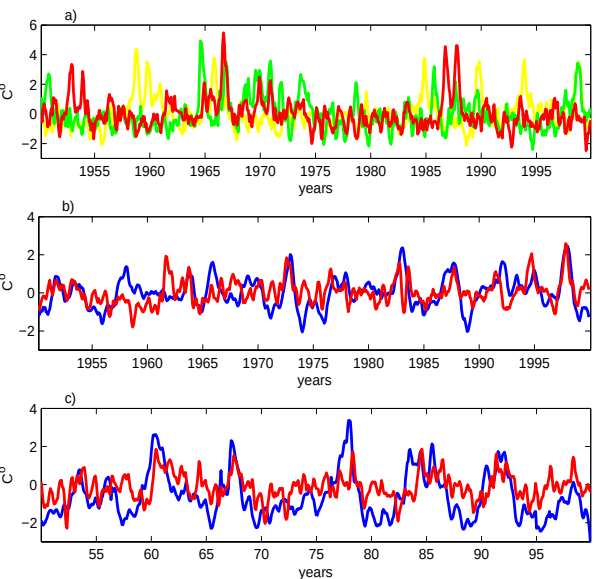
a)
6
4
2
0
−2
C°
1955
1960
1965
1970
1975
1980
1985
1990
1995
years
b)
4
2
0
−2
C°
1955
1960
1965
1970
1975
1980
1985
1990
1995
years
c)
4
2
0
−2
C°
55
60
65
70
75
80
85
90
95
years

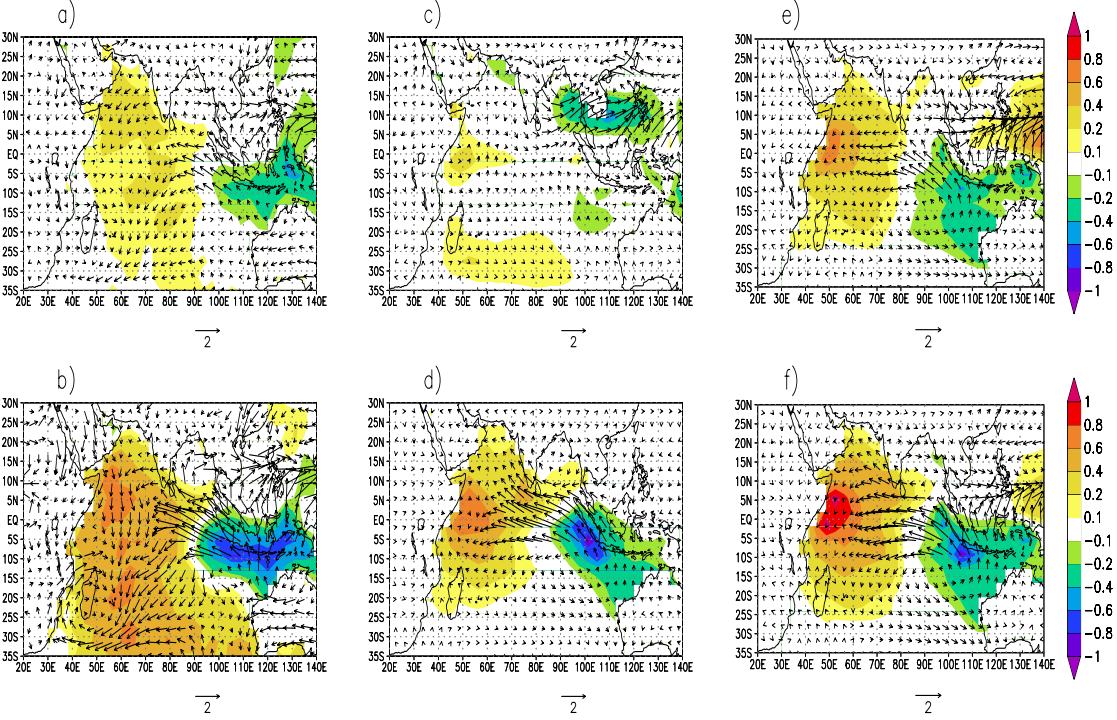
a)
c)
e)
b)
d)
f)
30N 25N 20N 15N 10N 5N EQ 5S 10S 15S 20S 25S 30S 35S
20E 30E 40E 50E 60E 70E 80E 90E 100E 110E 120E 130E 140E
2
1
0.8
0.6
0.4
0.2
0.1
−0.1
−0.2
−0.4
−0.6
−0.8
−1

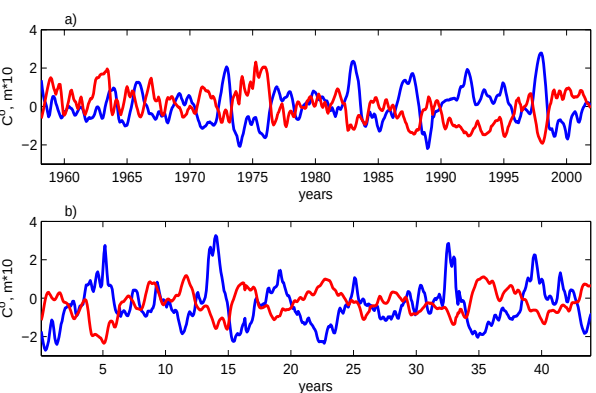
a)
4
2
0
−2
C^0, m*10
1960
1965
1970
1975
1980
1985
1990
1995
2000
years
b)
4
2
0
−2
C^0, m*10
5
10
15
20
25
30
35
40
years